Waveform and Space Precoding for Next Generation Downlink Narrowband IoT

Tongyang Xu, *Member, IEEE*, Christos Masouros, *Senior Member, IEEE*, and Izzat Darwazeh, *Senior Member, IEEE*

***Abstract*—Narrowband Internet of Things (NB-IoT) was introduced by 3GPP in low power wide area network to support low power and wide coverage applications. Since it follows long term evolution standard, its signal quality is guaranteed and its deployment is straightforward via reusing existing infrastructures. Current NB-IoT supports low data rate services via using low order modulation formats for the purpose of power saving. However, with the increase of data rate driven applications, next generation NB-IoT would require data rate enhancement techniques without consuming extra battery power. In this paper, a downlink framework, using a nonorthogonal signal waveform for next generation enhanced NB-IoT (eNB-IoT), is proposed and experimentally tested in both single-antenna and multiantenna systems. In the single-antenna scenario, waveform precoding is used to pre-equalize the self-created inter carrier interference distorted signal waveform. For the multiantenna multiuser scenario, both waveform and antenna space precoding have to be used. Measured results show that in both single-antenna and multiantenna systems, the proposed signal waveform in eNB-IoT can increase data rate by ∼11% compared with NB-IoT occupying the same spectral resource in similar receiver computational complexity.**

***Index Terms*—Enhanced narrowband Internet of Things (eNB-IoT), multiantenna, multiple input multiple output (MIMO), multiuser, narrowband 5G, NB-IoT, nonorthogonal, precoding, prototyping, software defined radio (SDR), waveform**

I. Introduction

NARROWBAND Internet of Things (NB-IoT) [1] is a cellular IoT technique standardized in 3GPP. It provides quality guaranteed services due to its paid spectral license. Unlike other IoT techniques, such as LoRa [2] and SigFox [3], NB-IoT employs multicarrier signal waveform and is compatible with fourth generation long term evolution networks. Therefore, its deployment is straightforward [4] and it is becoming quite important in many IoT-based applications and it leads the way for future narrowband fifth generation.

The downlink signal of NB-IoT occupies 12 subcarriers with total bandwidth of 180 kHz. Its uplink channel supports either multicarrier waveform or single-tone waveform. Due to its narrow band characteristic, NB-IoT can cover a wide communication range [5]. NB-IoT has been standardized and its commercialized chip has been released with a reasonable price. However, with the ever-increasing requirements and the need to accommodate emerging applications, existing NB-IoT is approaching its limit owing to a number of factors.

1) Pressure of massive IoT data. More IoT devices are being connected in networks due to emerging applications.
2) Shortage of spectral resources. Each NB-IoT signal occupies bandwidth of 180 kHz, and this is becoming a limiting factor to NB-IoT.
3) Insufficient data rate. Maximum modulation format in NB-IoT is quadrature phase-shift keying (QPSK), which is not sufficient for data rate driven applications.
4) High power consumption. To achieve a wide signal coverage, repetitive transmission is employed but with the challenge of extra power consumption.

Therefore, the upgrade to next generation enhanced NB-IoT (eNB-IoT) is necessary. In order to enhance existing NB-IoT, it is crucial to develop new spectrum and power efficient communication techniques. Waveform design is an efficient solution to lead the narrowband 5G. Previous work in [6]–[9] has presented solutions for eNB-IoT using spectrally efficient frequency division multiplexing (SEFDM) [6], Half-Sinc [7], and fast-orthogonal frequency division multiplexing (Fast-OFDM) [8], [9] nonorthogonal signal waveforms and brings benefits against conventional orthogonal frequency division multiplexing (OFDM), such as follows.

1) Improve data rate without upgrading modulation formats [6], [7].
2) Double the number of connected IoT devices without occupying extra spectral resources [8].
3) Extend signal coverage using a power efficient waveform scheduling scheme [9].

Applications of SEFDM have been explored in different areas, such as visible light communication [10], [11], optical systems [12]–[14], mm-wave [15], spectral and energy efficiency [16], and capacity gains [17]. However, due to the nonorthogonally packed subcarriers in SEFDM, self-created inter carrier interference (ICI) is introduced and power consuming signal processing is required at the receiver. Therefore, it is suitable for uplink channel since the signal processing is at base stations [6]. For downlink channels, this necessitates extra receive processing at the IoT devices which renders it

Manuscript received December 17, 2018; revised January 05, 2019; accepted January 22, 2019. Date of publication January 31, 2019; date of current version June 19, 2019. This work was supported in part by the Engineering and Physical Sciences Research Council "Impact Acceleration Discovery to Use" Award under Grant EP/R511638/1, and in part by National Instruments. *(Corresponding author: Tongyang Xu.)*

The authors are with the Department of Electronic and Electrical Engineering, University College London, London WC1E 7JE, U.K. (e-mail: tongyang.xu.11@ucl.ac.uk; c.masouros@ucl.ac.uk; i.darwazeh@ucl.ac.uk).

Digital Object Identifier 10.1109/JIOT.2019.2896724

impractical. Battery power is a critical factor in NB-IoT. As surveyed by [18], the battery life of an NB-IoT device is designed to last at least ten years without battery replacement. In this case, each device has to be designed power efficiently. Therefore, the signal processing has to be as simple as possible. Thus, in order to evolve to narrowband 5G for the downlink channel, power efficient precoding techniques have to be used together with waveform design.

This paper details the design and testing of the nonorthogonal SEFDM waveform in both single-antenna and multiantenna systems to enhance the downlink data rate for next generation eNB-IoT. A joint two-stage waveform and space precoding architecture is proposed. The waveform precoding is to pre-equalize the self-created ICI within the waveform and the space precoding is to precancel the multiantenna multiuser spatial interference. This paper practically sets up a world-first real-time multiantenna multiuser nonorthogonal waveform IoT experiment operating on a realistic over-the-air multiple input multiple output (MIMO)-SEFDM transmission link. Measured results, on a software defined radio (SDR) testbed, verifies that the waveform precoding and space precoding can efficiently precancel waveform interference and antenna spatial interference at the transmitter, respectively. Moreover, the collected data from the MIMO-SEFDM SDR testbed demonstrates that the proposed nonorthogonal waveform for eNB-IoT can increase data rate by $\sim$11% than NB-IoT while occupying the same spectral resource and in the similar receiver computational complexity.

II. Waveform Design and Its Benefits

There are mainly two groups of nonorthogonal waveforms. One is the bandwidth compressed multicarrier waveform including Fast-OFDM [19], SEFDM [20], and Half-Sinc [7]. The other one is the out-of-band power suppression waveform including filterbank-based multicarrier [21], generalized frequency division multiplexing [22], and universal-filtered multicarrier [23]. The first group focuses on compressing occupied spectral bandwidth while maintaining the same data rate or occupying the same spectral bandwidth but with improved data rate. The second group can suppress the out-of-band power leakage leading to closer signal band packing without co-band interference. This paper focuses on the bandwidth compressed SEFDM waveform since it can be flexibly configured for different applications. In addition, work in [24] verified that the waveform shaping can also be applied to the bandwidth compressed signals.

Subcarrier allocation schemes for both OFDM and SEFDM are illustrated in Fig. 1. The first figure shows the typical OFDM subcarrier packing scheme, where 12 subcarriers are orthogonally packed with no interference. For SEFDM, two advantages can be achieved in either bandwidth saving or data rate improvement. The original idea of the SEFDM signal waveform is to pack subcarriers closer in the frequency domain, thus signal bandwidth is compressed as shown in Fig. 1, which is "SEFDM Type-I." Its benefit is to transmit the same amount of data while occupying narrower bandwidth. In this case, the noise power is reduced within a narrower signal

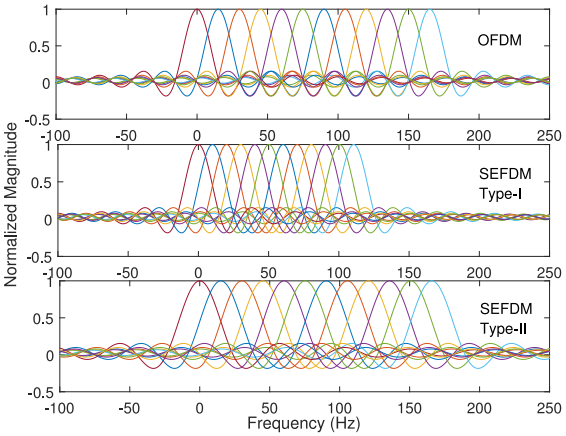

Fig. 1. Subcarrier allocation schemes for different multicarrier signals. OFDM (12 subcarriers, data rate is R_b). SEFDM Type-I (12 subcarriers, bandwidth compression factor α, data rate is R_b). SEFDM Type-II (12 subcarriers, bandwidth compression factor α, data rate is R_b/α).

band and the saved bandwidth could be reserved for extra IoT devices. It should be noted that this paper is aimed at future IoT communications. Therefore, the subcarrier spacing of SEFDM signals may be not consistent with existing 3GPP standards. Based on the Type-I signal waveform, a data rate improved "SEFDM Type-II" waveform is proposed to increase data rate per subcarrier while maintaining the same occupied signal bandwidth. Compared with the OFDM signal waveform, the overall bandwidth is the same while the bandwidth of each subcarrier is wider. In this case, using the same number of subcarriers with a higher data rate per subcarrier, the overall signal data rate is improved. In this paper, we will focus on the SEFDM Type-II signal waveform, which can enhance the data rate for next generation eNB-IoT applications.

A. Signal Waveform Model

In a system with N subcarriers, the discrete SEFDM signal is mathematically represented by

$$X_k = \frac{1}{\sqrt{N}} \sum_{n=1}^{N} s_n \exp\left(\frac{j2\pi nk\alpha}{N}\right) \tag{1}$$

where X_k is the kth time sample with $k = [1, \ldots, N]$, $\alpha = \Delta f \cdot T$ is the bandwidth compression factor, where Δf denotes the subcarrier spacing and T is the period of one SEFDM symbol. Thus, the percentage of bandwidth saving is equal to $(1-\alpha) \times 100\%$. s_n is a complex symbol modulated on the nth subcarrier and $(1/\sqrt{N})$ is a scaling factor.

The matrix form of the discrete SEFDM signal is expressed as

$$X = \mathbf{F}S \tag{2}$$

where S is an N-dimensional vector of transmitted complex symbols, X is an N-dimensional vector of SEFDM time samples, and $\mathbf{F}$ is an $N \times N$ subcarrier matrix with elements equal to $e^{(j2\pi nk\alpha/N)}$.

To simplify the signal waveform modeling, channel effect is not taken into account in the model. Therefore, the transmitted signal is only distorted by additive white Gaussian noise

(AWGN) Z. At the receiver, the contaminated signal is demodulated by multiplying with the conjugate subcarrier matrix $\mathbf{F}^*$ with elements equal to $e^{(-j2\pi nk\alpha/N)}$. The demodulation is expressed as

$$R = \mathbf{F}^*(X+Z) = \mathbf{F}^*\mathbf{F}S + \mathbf{F}^*Z = \mathbf{C}S + Z_{\mathbf{F}^*} \tag{3}$$

where R is an N-dimensional vector of demodulated symbols, $Z_{\mathbf{F}^*}$ is the AWGN demodulated by the conjugate subcarrier matrix $\mathbf{F}^*$ and $\mathbf{C}$ is an $N \times N$ correlation matrix equals to $\mathbf{C} = \mathbf{F}^*\mathbf{F}$ whose elements are defined as

$$\begin{aligned} c_{m,n} &= \frac{1}{N}\sum_{k=1}^{N} e^{\frac{j2\pi mk\alpha}{N}} e^{-\frac{j2\pi nk\alpha}{N}} \\ &= \begin{cases} 1, & m = n \\ \dfrac{1 - e^{j2\pi\alpha(m-n)}}{N\left(1 - e^{\frac{j2\pi\alpha(m-n)}{N}}\right)}, & m \neq n \end{cases} \end{aligned} \tag{4}$$

where m,n are indices of two arbitrary subcarriers. The diagonal elements ($m = n$) indicate constructive auto-correlation while the nondiagonal nonzero elements ($m \neq n$) represent destructive cross-correlation ICI.

B. Signal Generation and Demodulation

The signal can be generated directly using (1) at the expense of high computational complexity. However, in order to make use of the efficient inverse fast Fourier transform (IFFT) algorithm, a proper signal generation approach has to be designed for SEFDM.

The basic idea is to pad zeros at the end of each input QAM symbol vector. The length of a new QAM symbol vector becomes $M = N/\alpha$. Therefore, it is possible to use a single IFFT of length N/α for simplified signal generation. The zero padding is operated as

$$s'_i = \begin{cases} s_i, & 1 \leq i \leq N \\ 0, & N < i \leq M. \end{cases} \tag{5}$$

Therefore, the new form of the SEFDM signal is expressed as

$$X'_k = \frac{1}{\sqrt{M}}\sum_{n=1}^{M} s'_n \exp\left(\frac{j2\pi nk}{M}\right) \tag{6}$$

where $n, k = [1, \ldots, M]$. The output symbol vector X' of a M length is truncated with the first N samples reserved while the rest is discarded.

It should be noted that the signal demodulation at the receiver is the reverse operation of the signal generation at the transmitter. Thus, the signal demodulation can be realized efficiently via the zero padding method as well.

C. PAPR Comparison

The dynamic range of a signal determines the dynamic range of a component and peak-to-average power ratio (PAPR) is used to measure the variation of signal power. The cumulative distribution function (CDF) is used as a way to analyze the probability of PAPR being smaller than a predefined threshold γ. Assume a signal $x(t)$ is obtained after the final stage of digital signal processing and the calculation of PAPR is given as

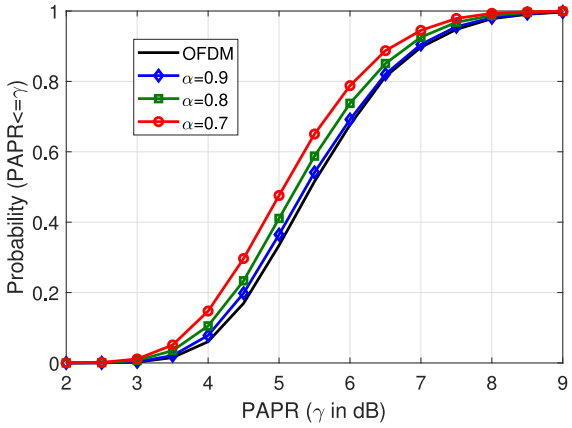

Fig. 2. CDF of PAPR for OFDM and SEFDM signal waveforms modulated by 4QAM symbols.

$$\text{PAPR} = \frac{\max|x(t)|^2}{E\left[|x(t)|^2\right]} \tag{7}$$

where $\max|x(t)|^2$ indicates the peak power of the signal $x(t)$, $E[.]$ is the expectation operator and $E[|x(t)|^2]$ denotes the average power.

Fig. 2 presents PAPR of four systems using the same number of subcarriers. One system is the typical OFDM with 4QAM modulation format. The other three systems are the SEFDM with 4QAM at different α. Results indicate that the probability of PAPR below and equal the threshold γ of SEFDM is better than that of OFDM. It should be noted that the PAPR performance of SEFDM is improved with the reduction of α.

III. System Architectures and Precoding

A. System Architecture

To simplify signal processing of each IoT device, precoding is used to precancel interference at the transmitter and therefore the signals at each IoT device can be recovered directly. The ICI is known at the transmitter when the SEFDM waveform is deterministically configured. Thus, the simple zero forcing (ZF) [25] waveform precoding method can be used at the transmitter based on the direct ICI matrix inversion. In multiantenna scenarios, multiple antennas will transmit different signals simultaneously resulting in interference to each receiver user. The linear ZF [25] MIMO space precoding can be used for spatial antenna interference cancelation at the transmitter based on the feedback channel state information (CSI).

System architectures for the downlink eNB-IoT in both single-antenna and multiantenna scenarios have to be redesigned with either one-stage precoding or two-stage precoding schemes, as illustrated in Fig. 3.

In a single-antenna single-user SEFDM eNB-IoT system shown in Fig. 3(a), a waveform precoding module is used before IFFT to precancel the self-created ICI. For a typical

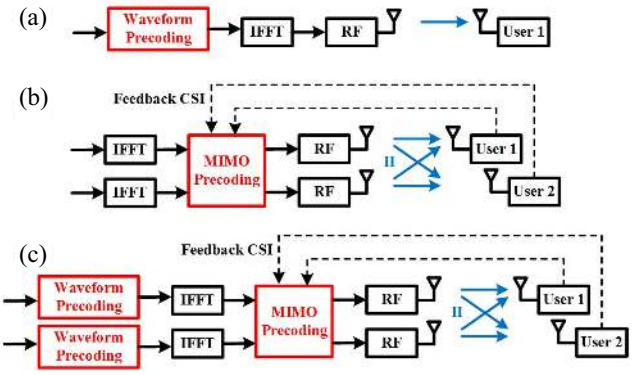

Fig. 3. Architectures of precoding SISO and precoding MU-MIMO systems for (a) one-stage precoding SISO-SEFDM-based eNB-IoT, (b) one-stage precoding MU-MIMO-OFDM-based NB-IoT, and (c) two-stage precoding MU-MIMO-SEFDM-based eNB-IoT.

OFDM NB-IoT system, the waveform precoding module is removed since there is no ICI.

In an MU-MIMO-OFDM-based NB-IoT system shown in Fig. 3(b), an MIMO precoding module is included. For simplicity, we use two antennas and two users for explanation. Each antenna is responsible for one OFDM symbol stream. Thus, two IFFT modules are needed at the transmitter. The data from each antenna will interfere with each other due to the MIMO channel $\mathbf{H}$ and each user antenna will receive interfered data from both transmitter antennas. The MIMO precoding module is applied to precancel the antenna spatial interference at the transmitter based on the feedback CSI. Therefore, the user antennas will receive interference free data. The main benefit of this MIMO precoding architecture is that each receiver is simplified and can process data independently. Therefore, it is suitable for downlink IoT scenarios.

For multiuser MIMO (MU-MIMO)-SEFDM-based eNB-IoT, as explained in Section II, the resulting interference consists of both antenna spatial interference and the self-created ICI. Following the same system architecture in Fig. 3(b), antenna spatial interference can be removed but the signal internal ICI still exists. Therefore, a two-stage precoding architecture for eNB-IoT is designed and presented in Fig. 3(c). The system architecture partially follows the MU-MIMO-OFDM but with a waveform precoding module added before each IFFT. Since the waveform characteristic is predefined in the correlation matrix $\mathbf{C}$, therefore the waveform precoding is operated based on the known correlation matrix without any feedback information from the receiver. Thus, the two-stage precoding can efficiently remove antenna spatial interference and SEFDM waveform internal ICI leading to a simple receiver design for eNB-IoT.

B. Waveform Precoding

The basic principle of the waveform precoding is to precancel waveform self-created ICI. This concept can be used in any waveforms when the waveform characteristic is deterministic. In this paper, we focus on SEFDM, which has predefined self-created ICI information in the matrix $\mathbf{C}$. As is shown in (2), transmitted symbols are modulated on a multicarrier signal via multiplying with the subcarrier matrix $\mathbf{F}$. For the precoding operation, the raw symbols are premultiplied with the inverse of the matrix $\mathbf{C}$ before modulation. Therefore, the idea is to equalize the symbols on each subcarrier based on the predefined precoding matrix $\mathbf{C_p}$ as the following:

$$\mathbf{C_p} = \mathbf{C}^H\left(\mathbf{C}\mathbf{C}^H\right)^{-1}. \tag{8}$$

Thus, the precoded signal $\bar{S}$ is defined as

$$\bar{S} = \mathbf{C_p}S. \tag{9}$$

Then the precoded SEFDM signal is expressed as

$$\bar{X} = \mathbf{F}\bar{S}. \tag{10}$$

Following the same operation from (2) to (3), the newly demodulated signal at the receiver is expressed as

$$\begin{aligned} R &= \mathbf{F}^*\left(\bar{X} + Z\right) \\ &= \mathbf{F}^*\mathbf{F}\bar{S} + \mathbf{F}^*Z \\ &= \mathbf{C}\mathbf{C_p}S + Z_{\mathbf{F}^*} \\ &= \hat{S} + Z_{\mathbf{F}^*} \end{aligned} \tag{11}$$

where $\hat{S}$ is the demodulated symbols at the receiver. The precoding operation is similar to the one in MIMO systems [26]. However, the precoding matrix in SEFDM is deterministic and no feedback information is required.

C. MIMO Precoding

To avoid spatial interference from different antennas, we use time orthogonal pilot symbols to measure channel conditions. Since the system is not in a massive size in this paper, the base station will send time orthogonal pilot symbols to multiple users at the same time. Each user will receive their own allocated pilot symbols without co-user interference. Each user independently estimates CSI and sends it back to the base station for precoding.

To explain the precoding operation in a simple way, we assume a two-antenna two-user scenario as illustrated in Fig. 3(b) and (c). The channel matrix $\mathbf{H}$ is therefore defined as

$$\mathbf{H} = \begin{bmatrix} h_{11} & h_{12} \\ h_{21} & h_{22} \end{bmatrix}. \tag{12}$$

The designed time orthogonal pilot symbols are sent from two transmit antennas over two symbol periods. In the first time period, the first antenna sends symbol p_1 while the second antenna sends nothing. In the second time period, the first antenna sends nothing while the second antenna sends symbol p_2. In this case, spatial interference from two antennas can be avoided. The matrix form of the time orthogonal pilot symbols is expressed as

$$\mathbf{P} = \begin{bmatrix} p_1 & 0 \\ 0 & p_2 \end{bmatrix}. \tag{13}$$

Thus, the received symbols from two antennas at the receiver are given by

$$\begin{bmatrix} y_{11} & y_{12} \\ y_{21} & y_{22} \end{bmatrix} = \begin{bmatrix} h_{11} & h_{12} \\ h_{21} & h_{22} \end{bmatrix} \times \begin{bmatrix} p_1 & 0 \\ 0 & p_2 \end{bmatrix} + \begin{bmatrix} z_1 \\ z_2 \end{bmatrix} \tag{14}$$

where y_{11} and y_{12} are the received symbols on the first antenna at the first time period and the second time period, respectively. The two symbols y_{21} and y_{22} are received on the second

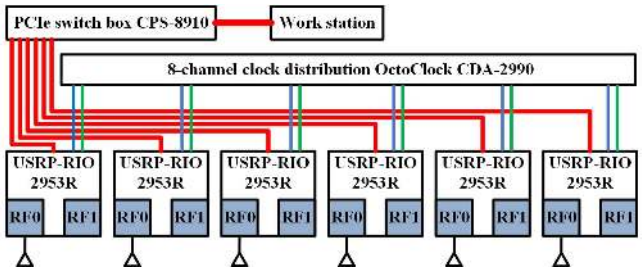

Fig. 4. System architecture and components connections. Red connections indicate NI MXI-Express Gen 2 ×8 cables. Blue connections indicate SMA cables delivering 10 MHz reference signals. Green connections indicate SMA cables delivering PPS signals.

antenna. z_1 and z_2 are AWGN on the first and second antennas, respectively. Therefore, we can derive the channel condition information in the following:

$$\hat{\mathbf{H}} = \begin{bmatrix} \hat{h}_{11} & \hat{h}_{12} \\ \hat{h}_{21} & \hat{h}_{22} \end{bmatrix} = \begin{bmatrix} y_{11}/p_1 & y_{12}/p_2 \\ y_{21}/p_1 & y_{22}/p_2 \end{bmatrix}. \tag{15}$$

Since the antenna spatial information $\hat{\mathbf{H}}$ is estimated, the data symbols $\tilde{X}$ from two antennas in one time period are precoded and expressed in matrix form as

$$\bar{Y} = \hat{\mathbf{H}}_{\mathbf{p}}\tilde{X} = \hat{\mathbf{H}}^H\left(\hat{\mathbf{H}}\hat{\mathbf{H}}^H\right)^{-1}\tilde{X} \tag{16}$$

where $\bar{Y} = [\bar{y}_{11}, \bar{y}_{21}]$ indicates MIMO precoded signals from two antennas and $\tilde{X} = [\bar{x}_{11}, \bar{x}_{21}]$ represents precoded waveform signals from two antennas. It should be noted that $\bar{x}$ is one sample in one SEFDM signal $\bar{X}$ derived in (10) and $\bar{x}_{11}$ indicates the first sample of an SEFDM signal from the first antenna while $\bar{x}_{21}$ is the first sample of an SEFDM signal from the second antenna.

IV. Experiment Design and System Implementation

A. Platform Setup

The system architecture and its components connections are shown in Fig. 4. The experiment is designed for proof-of-concept of the downlink multiuser eNB-IoT. Therefore, we are not considering massive multiple input multiple output (MIMO) [27], [28] but a simple system with six transmission antennas in a realistic indoor wireless environment. For simplicity, we only test a two user case. The channel is time-invariant and no obvious Doppler issues exist since each IoT device is stationary after deployment. We use six NI USRP-RIO 2953R SDR devices to emulate the transmitter and user functions. Each device has two separate and independent RF chains, in which the fist RF chain is for signal transmission and the other one is for signal reception.

In order to synchronize six USRPs in both frequency and time, a CDA-2990 8-channel clock distribution OctoClock module is used. It can split and amplify a 10 MHz reference signal and a pulse per second (PPS) signal to support up to eight USRPs. Raw digital data is generated by LabVIEW in a control host and is sent to a cabled PCI-express switch box CPS-8910 via an NI MXI-Express Gen 2 ×8 Cable, which can support up to 3.2 GB/s. The switch box separates the serial data to six data streams, which are sent to six USRPs in parallel. Omni-directional antennas are used in the testbed to verify the precoding feasibility. The realistic experiment testbed operating at 2.4 GHz is presented in Fig. 5 with key system parameters shown in Table I. It should be noted that the SEFDM Type-II signal, shown in Fig. 1, is used in the experiment. Therefore, to maintain the similar signal bandwidth while achieving higher data rate, the sampling rate for eNB-IoT is higher than that of NB-IoT. Furthermore, for a fair comparison of performance we choose $\alpha = 0.9$ so that the SEFDM and OFDM signals have almost equal PAPR as shown in Fig. 2. The control host, illustrated in Fig. 6, is a computer, which can control the USRP array, such as sending and receiving data from antennas.

TABLE I
System Specifications

Parameter	NB − IoT	eNB − IoT
No. of BS antennas	6	6
No. of users	2	2
RF center frequency (GHz)	2.4	2.4
Sampling frequency (MHz)	1.92	2.13
FFT size	128	128
No. of guard band sub-carriers	58	58
No. of data sub-carriers	12	12
No. of cyclic prefix samples	10	10
Bandwidth (kHz)	180	180

Fig. 5. Base station (USRP array).

Fig. 6. Control host.

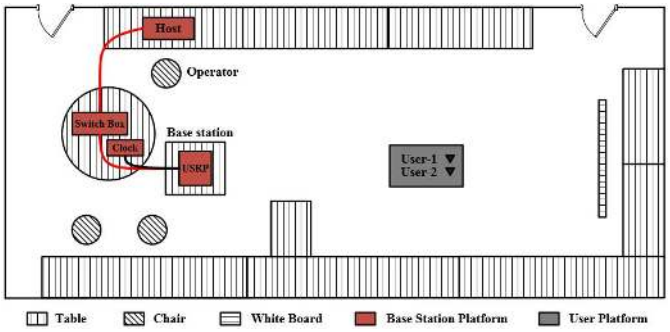

Fig. 7. Indoor floor plan and the location of USRP base station (has Tx antennas), user IoT devices (has Rx antennas), control host and experiment operator. The laboratory is around 9 m long and 4 m wide.

Fig. 8. User antennas (user 1 and user 2).

The floor plan of the control host, base station, and user antennas are illustrated in Fig. 7. The floor plan shows the simplified illustration of the experiment setup. Other unnecessary equipments and objects are skipped in this illustration. The user antennas in this experiment are labeled with black triangular blocks. For proof-of-concept purposes, two user antennas (Rx antennas), shown in Fig. 8, are placed in random locations in a room but in line of sight of the base station USRP array, which has six Tx antennas. Distances are varied from a fraction of one meter to around half length of the room which was close to 5 m. For a worst case scenario the two user antennas are placed very closely together and spaced by only 10 cm. For a realistic and better determined path loss and noise modeling for different receiver signal-to-noise ratio (SNR) values, a channel emulator (Spirent VR5) is used as described in Section V-C.

B. Frame Structure

The overhead for frame timing synchronization is not included in the frame structure. The reason is that the experiment is designed for proof-of-concept and it continuously sends and receives signals for the testing. Once the frame is synchronized, the following data frames will not need the frame timing sequence any more. Therefore, we remove this kind of overhead, which is only used once in this experiment.

In this paper, the base station is assumed to have six antennas and provide services to two users. The downlink signal is generated in the base station with a designed frame structure and resource block structure illustrated in Fig. 9. The 10 ms frame is divided into 20 time slots with each one occupies 0.5 ms. The first time slot is reserved for downlink antenna spatial CSI estimation. All the other time slots ranging from 01 to 19 are used for data transmission. Each time slot has seven OFDM/SEFDM symbols as shown in the figure. In order to avoid interference between antennas, the overhead of spatial CSI estimation for each antenna is interleaved at different symbol locations in time. The CSI estimation overhead from the first antenna occupies the first OFDM symbol in one resource block while keeping blank for the following five OFDM/SEFDM symbols, which are reserved for the rest five antennas. All the other five antennas follow the same principle to avoid the overlapping interference. The last OFDM/SEFDM symbol in one resource block from all the six antennas is reserved for the downlink pilos, which are used to compensate for imperfect channel issues, such as power normalization and imperfect timing and phase synchronization [29]. The downlink pilots from all the six antennas are precoded and sent simultaneously. It should be noted that the system is robust to oscillator variation [30] even under the self-created ICI.

In order to get accurate downlink spatial CSI estimate for each antenna, a time-domain orthogonal sounding reference signal (SRS) is used. Thus, antenna spatial interference can be avoided. The SRS frame structure is shown in Fig. 9. Since the SRSs are interleaved and sent over the air, each user will receive staggered SRS from all of the transmitter antennas. The estimated downlink antenna spatial CSI will be feedback to the transmitter for space precoding. The precoding method used in this paper is in the time-domain, where the channel is assumed to be stable within one OFDM/SEFDM frame transmission. Since we are focusing on a system with six transmitter antennas, therefore, each user just needs to feedback six CSI coefficients and the overhead length is reasonable. In addition, due to the robustness to multipath effect in OFDM/SEFDM, the compensation of this effect is operated at the receiver via the simple one-tap equalizer [31].

It should be noted that in nonfeedback systems, CSI is obtained based on the channel reciprocity. In addition, multipath effect exists in a practical over-the-air transmission scenario. Therefore, precoding has to be operated on each subcarrier in the frequency-domain with extra signal processing, such as CSI interpolation. However, realistic channels are not perfect reciprocity due to the time-variant analogy components and a lot of efforts have to be allocated to reciprocity calibration. Therefore, instead of using the nonfeedback system architecture, this paper employs a feedback system architecture for simplification of the next generation eNB-IoT.

V. Measured Results and Discussion

In this paper, we evaluate error vector magnitude (EVM) and bit error rate (BER) for received constellation diagrams together with data rate demonstrations. In terms of EVM calculation, we use the reference signal normalization method defined as

$$\mathrm{EVM} = \sqrt{\frac{\frac{1}{K}\sum_{i=0}^{K-1}\left(\left(I_i - \bar{I}_i\right)^2 + \left(Q_i - \bar{Q}_i\right)^2\right)}{\frac{1}{K}\sum_{i=0}^{K-1}\left((I_i)^2 + (Q_i)^2\right)}} \tag{17}$$

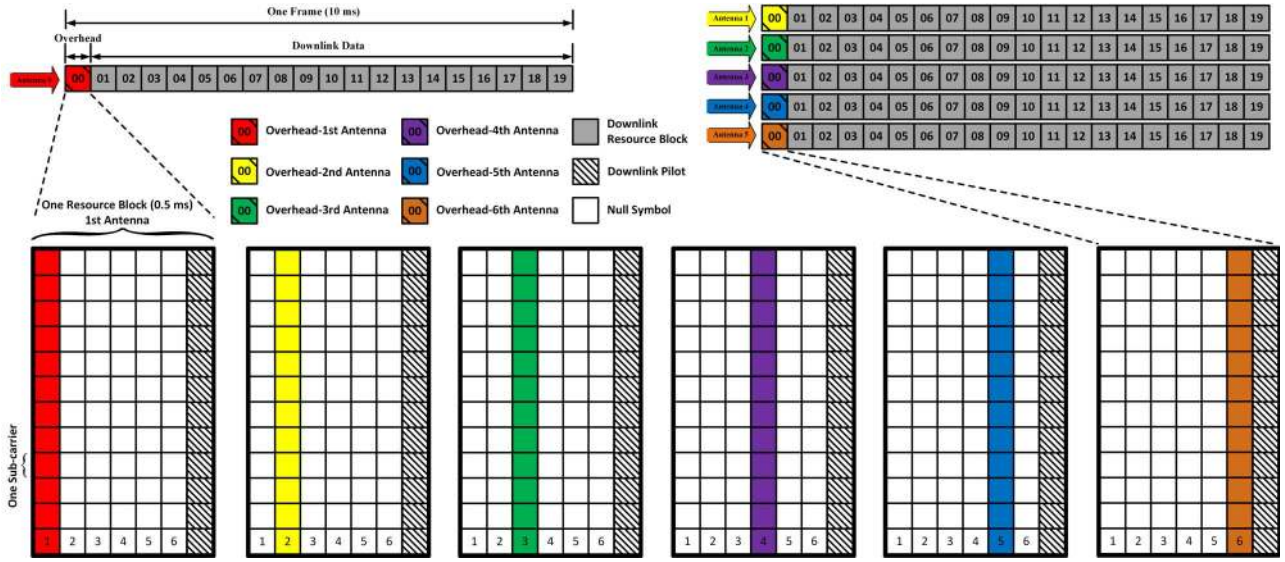

Fig. 9. Frame and resource block structure for each antenna. One frame consists of 20 time slots and the first time slot is the overhead including SRS for downlink antenna spatial CSI estimation, which is used for space precoding at the transmitter. The locations of overhead from different antennas are staggered to avoid interference.

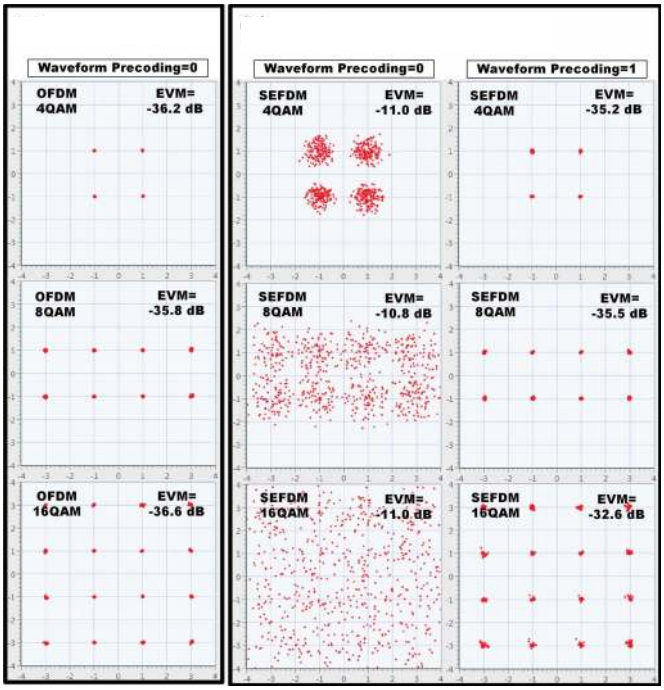

(a) (b)

Fig. 10. Measured constellation diagrams with normalized EVM performance in SISO systems. "Waveform Precoding=1" indicates SEFDM self-created ICI precoding is enabled. (a) SISO-OFDM and (b) SISO-SEFDM.

where I_i and Q_i are the ith reference in-phase and quadrature symbols, respectively. $\bar{I}_i$ and $\bar{Q}_i$ are the ith measured in-phase and quadrature symbols, respectively. K represents the number of symbols used in the EVM calculation.

A. Single-Antenna Single-User

First, we test the typical "SISO-OFDM"-based NB-IoT performance in Fig. 10(a). Then, we test single-antenna single-user eNB-IoT performance, which is noted as "SISO-SEFDM" in Fig. 10(b). The SISO-SEFDM experiment is operated on the same testbed shown in Fig. 5. It should be noted that in order to realize a single-antenna single-user signal transmission, it is straightforward to reconfigure the testbed by blocking five transmitter antennas while transmitting signals on one antenna at the base station. In addition, only one user antenna is maintained for signal reception. Therefore, the single-input single-output (SISO) system architecture follows Fig. 3(a).

Three modulation formats are tested ranging from 4QAM to 16QAM. In a standard NB-IoT system, the maximum supported modulation format is 4QAM (QPSK). For future potential evolutions, it is not clear whether higher order modulation schemes would be considered or not. Therefore, we explore the upper limit of our proposed eNB-IoT with various modulation formats up to 16QAM. As is shown in Fig. 10(b), two systems are tested. The column with "Waveform Precoding = 0" indicates no precoding is applied to SEFDM signals. Thus, due to the self-created ICI, the receiver cannot recover the signal properly. It is clearly seen that the constellation points are significantly scattered for various modulation formats. However, applying the waveform precoding in Section III-B, the quality of constellation is greatly improved as shown in the second column in Fig. 10(b).

It should be noted that with the waveform precoding, the SISO-SEFDM can achieve similar EVM performance as the typical SISO-OFDM, for 4QAM and 8QAM. However, for 16QAM, SISO-SEFDM is 5 dB worse than the SISO-OFDM. The reason for this could be the high constellation density of 16QAM, which challenges the waveform precoding.

B. Multiantenna Multiuser

With multiple antennas included in the system, the spatial interference is introduced and each received data stream

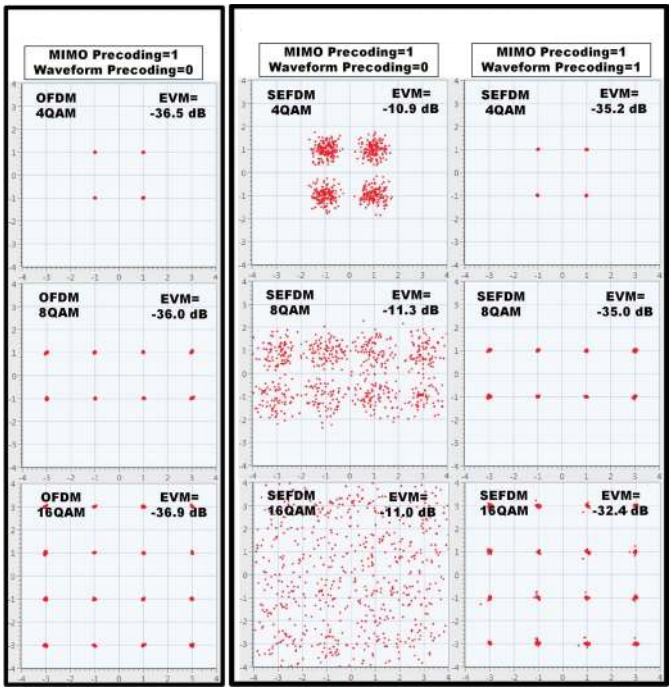

(a) (b)

Fig. 11. Measured constellation diagrams with normalized EVM performance in MU-MIMO systems. "MIMO Precoding=1" indicates the antenna spatial interference precoding is enabled. Waveform Precoding=1 indicates SEFDM self-created ICI precoding is enabled. (a) MU-MIMO-OFDM and (b) MU-MIMO-SEFDM.

is interfered by other parallel signals. Due to the subcarrier orthogonality in OFDM, the performance can be guaranteed without any waveform precoding methods. However, without proper antenna spatial interference cancelation, the signal cannot be easily recovered and the constellation would be greatly interfered. With the MIMO precoding, the spatial interference can be mitigated and clean constellation points are obtained in Fig. 11(a).

For "MU-MIMO-SEFDM" signals, double interference is introduced and signals cannot be decoded properly with one stage precoding. The first column in Fig. 11(b) illustrates clearly that with the MIMO precoding, SEFDM signals can be partially recovered. It shows very similar constellation patterns as the SISO-SEFDM results in Fig. 10(b). However, with the waveform precoding, the self-created ICI within SEFDM can be removed. The constellation patterns after two stage precoding are shown in the second column in Fig. 10(b).

It should be noted that with the two stage precoding, the MU-MIMO-SEFDM can achieve similar EVM performance as the typical MU-MIMO-OFDM, for 4QAM and 8QAM but 5 dB worse than the MU-MIMO-OFDM for 16QAM. This discovery is similar to the SISO systems.

C. Bit Rate Evaluation

Effective bit rate, defined as the nonerror bits per second, is calculated in this section to show the benefit of using our designed nonorthogonal signal waveform. Since we are focusing on physical layer system design, the bit rate is calculated only related to the signal occupied bandwidth and BER. The effective bit rate is defined as follows:

$$R_e = (1 - \text{BER}) \times f_s \times \log_2 O \times (N_d/N), \tag{18}$$

where R_e is the effective bit rate, f_s is sampling rate, O is constellation cardinality, BER is the bit error rate, $(1 - \text{BER})$ indicates the probability of nonerror received bits, N_d is the number of data subcarriers and N is the number of total subcarriers.

TABLE II
DATA RATE COMPARISONS

Parameter	4QAM	8QAM	16QAM
NB-IoT (kbit/s)	360	540	720
eNB-IoT (kbit/s)	400	600	800

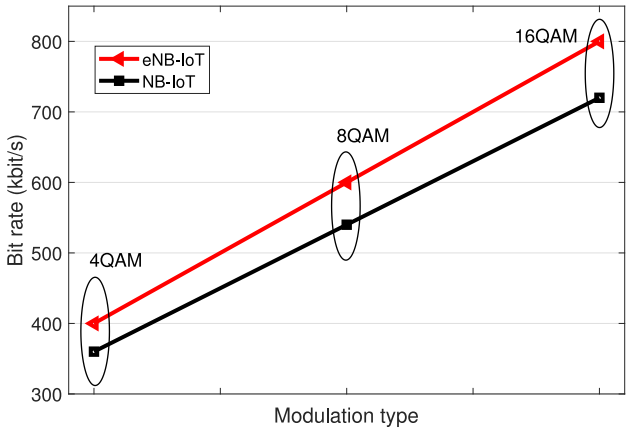

Fig. 12. Maximum bit rate comparison for both eNB-IoT and NB-IoT signal waveforms in different modulation schemes.

Table II summarizes the maximum bit rate for the two systems using different modulation schemes based on the calculation in (18). It should be noted that the BER, in the calculation, is set to zero. Therefore, $(1-\text{BER})$ is equal to "1" in this case. It is clearly seen that the data rate of eNB-IoT for different modulation schemes is improved by approximately 11% than that of NB-IoT. The data rate improvement is clearly illustrated in Fig. 12 as well.

Due to the limited indoor space, in order to test and compare NB-IoT and eNB-IoT at different SNR levels, a channel emulator VR5, shown in Fig. 13, is used to emulate noise and distort signals. We assume noise mainly comes from the receiver. Therefore, the two user antennas are connected to the VR5 via two cable extensions. By configuring the VR5, the path loss is set for each user and AWGN with various power levels is added to each received signal. According to the signal characteristics and the VR5 resolution limitations, the receiver bandwidth is set to 180 kHz and the AWGN bandwidth is set to 1.5625 MHz.

The power of transmitted signals from the base station antenna is -35 dBm and the receiver side signal power is set to -40 dBm. Thus, the path loss is 5 dB. Various noise power is configured in order to obtain different SNR values. The measured effective bit rates are therefore shown in Fig. 14. It is clearly seen that the BER performance collected from

Fig. 13. Channel emulator VR5 for path loss and noise emulation.

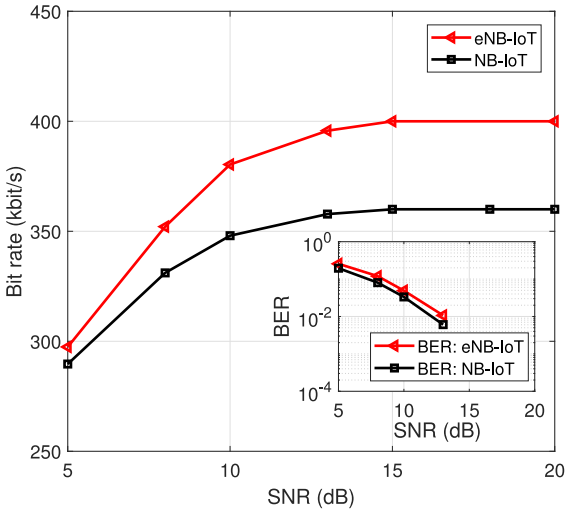

Fig. 14. Measured effective bit rates for both eNB-IoT and NB-IoT systems in 4QAM modulation formatted signals.

the testbed is very similar between the two systems with less than 1 dB gap at all BER levels. Based on the BER values and the calculation in (18), the effective bit rate of eNB-IoT, after SNR=15 dB, reaches 400 kbit/s while NB-IoT can only reach 360 kbit/s. The measured results verifies the theoretical conclusion in Fig. 12.

VI. Complexity Analysis for IoT Devices

This paper focuses on downlink system design. Therefore, the computational complexity is evaluated only for the receiver side IoT devices. The waveform and space precoding computations are at the transmitter and will not be taken into account as these are carried out at the base station which are typically more computationally resourceful. In addition, the feedback of CSI is not considered in the complexity comparison since it is assumed to be the same for both OFDM and SEFDM uplink channel signals. Therefore, the complexity comparison focuses only on the signal demodulation at the receiver. Since the signal demodulation is the reverse operation of the signal generation, the complexity analysis of signal demodulation would be similar to that of signal generation.

The direct operation is based on (1), where the multiplication of a vector and a matrix has to be computed resulting in high complexity. Then, the specially designed FFT method was described in Section II-B, where a single FFT can be used at the cost of larger FFT size. Furthermore, work in [32] proposed and implemented a pruned version of the single FFT demodulator. Its principle is to avoid zero operations. Thus, the system design is further simplified. Table III presents numerical results of complex multiplication and addition operations for OFDM and SEFDM systems. It should be noted that although the three SEFDM demodulation methods show different computational complexity, however, they lead to the same BER performance and therefore the same effective bit rate over the air.

TABLE III
Complexity in Terms of the Number of Complex Operations for OFDM and SEFDM Receiver Signal Demodulation

Operations	Multiplications	Additions
OFDM – FFT	$\frac{N}{2} \times log_2 N$	$N \times log_2 N$
SEFDM – Direct	N^2	$N \times (N-1)$
SEFDM – FFT	$\frac{N}{2\alpha} \times log_2 \frac{N}{\alpha}$	$\frac{N}{\alpha} \times log_2 \frac{N}{\alpha}$
SEFDM – Pruned – FFT	$\frac{N}{2\alpha} \times log_2 N$	$\frac{N}{\alpha} \times log_2 N$

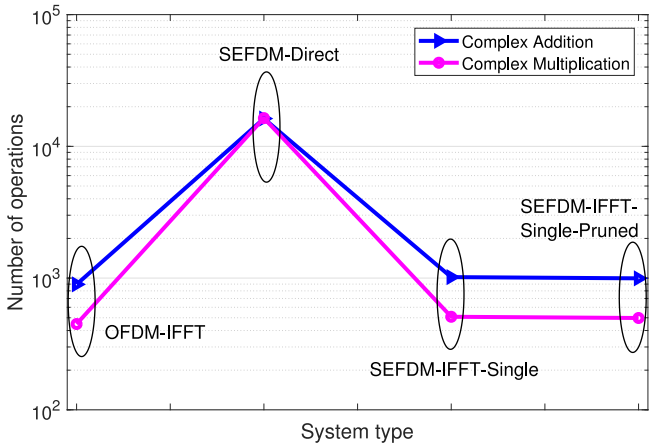

Fig. 15. Computational complexity in terms of complex addition and complex multiplication operations for different algorithms.

Fig. 15 illustrates the computational complexity of OFDM and SEFDM using different signal demodulation methods. First, it is noted that the numbers of complex additions for all the signal demodulation schemes are higher than that of complex multiplications. Furthermore, it is concluded from the figure that the direct operation of (1) results in the highest computational complexity for SEFDM while the single FFT and the pruned single FFT have similar computational complexity with OFDM.

VII. Conclusion

This paper proposed to use a nonorthogonal multicarrier SEFDM signal waveform to enhance the data rate for next generation eNB-IoT. The waveform packs subcarriers closer. Thus, with a higher sampling frequency, the data rate is improved while its occupied signal bandwidth is similar to the orthogonal OFDM waveform. Waveform precoding is used to

remove the self-created ICI within the nonorthogonal waveform. In addition, space precoding has to be used as well when multiple antennas are used. Measured EVM of different modulation schemes is first compared between different systems. Results showed that for modulation formats, such as 4QAM and 8QAM, eNB-IoT achieves the same performance as the NB-IoT in both single antenna and multiple antenna scenarios. For higher order modulation format, such as 16QAM, eNB-IoT performs slightly worse than NB-IoT due to its high constellation density. Effective bit rate is calculated based on practical BER values. Results showed that $\sim$11% data rate improvement is achieved using eN-IoT compared with NB-IoT in different modulation schemes. Furthermore, computational complexity of each system is calculated and compared in terms of complex multiplications and additions. Numerical results showed similar computational complexity of both eNB-IoT and NB-IoT. To summarize, the newly proposed eNB-IoT downlink framework can achieve $\sim$11% data rate improvement than NB-IoT with approximately the same receiver computational complexity.

REFERENCES

[1] R. Ratasuk, N. Mangalvedhe, Y. Zhang, M. Robert, and J.-P. Koskinen, "Overview of narrowband IoT in LTE Rel-13," in *Proc. IEEE Conf. Stand. Commun. Netw. (CSCN)*, Oct. 2016, pp. 1–7.

[2] N. Sornin, M. Luis, T. Eirich, T. Kramp, and O.Hersent, *LoRaWAN Specification, Version 1.0*, LoRa Alliance, Fremont, CA, USA, Jan. 2015.

[3] (Apr. 2018). *SigFox*. [Online]. Available: https://www.sigfox.com

[4] N. Mangalvedhe, R. Ratasuk, and A. Ghosh, "NB-IoT deployment study for low power wide area cellular IoT," in *Proc. IEEE 27th Annu. Int. Symp. Pers. Indoor Mobile Radio Commun. (PIMRC)*, Sep. 2016, pp. 1–6.

[5] M. Chen, Y. Miao, Y. Hao, and K. Hwang, "Narrow band Internet of Things," *IEEE Access*, vol. 5, pp. 20557–20577, 2017.

[6] T. Xu and I. Darwazeh, "Uplink narrowband IoT data rate improvement: Dense modulation formats or non-orthogonal signal waveforms?" in *Proc. IEEE 29th Annu. Int. Symp. Pers. Indoor Mobile Radio Commun. (PIMRC)*, Bologna, Italy, Sep. 2018, pp. 142–146.

[7] T. Xu and I. Darwazeh, "Half-Sinc waveform design for narrowband IoT," in *Proc. IEEE 29th Annu. Int. Symp. Pers. Indoor Mobile Radio Commun. (PIMRC)*, Sep. 2018, pp. 600–601.

[8] T. Xu and I. Darwazeh, "Non-orthogonal narrowband Internet of Things: A design for saving bandwidth and doubling the number of connected devices," *IEEE Internet Things J.*, vol. 5, no. 3, pp. 2120–2129, Jun. 2018.

[9] T. Xu and I. Darwazeh, "Non-orthogonal waveform scheduling for next generation narrowband IoT," in *Proc. IEEE Glob. Commun. Conf. Workshops Ultra High Speed Low Latency Massive Connectivity Commun. 5G/B5G (GC WS-UHS5G)*, Abu Dhabi, UAE, Dec. 2018.

[10] Y. Wang *et al.*, "SEFDM based spectrum compressed VLC system using RLS time-domain channel estimation and ID-FSD hybrid decoder," in *Proc. ECOC 42nd Eur. Conf. Opt. Commun.*, Sep. 2016, pp. 1–3.

[11] Y. Wang *et al.*, "Efficient MMSE-SQRD-based MIMO decoder for SEFDM-based 2.4-Gb/s-spectrum-compressed WDM VLC system," *IEEE Photon. J.*, vol. 8, no. 4, pp. 1–9, Aug. 2016.

[12] I. Darwazeh, T. Xu, T. Gui, Y. Bao, and Z. Li, "Optical SEFDM system; bandwidth saving using non-orthogonal sub-carriers," *IEEE Photon. Technol. Lett.*, vol. 26, no. 4, pp. 352–355, Feb. 15, 2014.

[13] J. Huang, Q. Sui, Z. Li, and F. Ji, "Experimental demonstration of 16-QAM DD-SEFDM with cascaded BPSK iterative detection," *IEEE Photon. J.*, vol. 8, no. 3, pp. 1–9, Jun. 2016.

[14] D. Nopchinda, T. Xu, R. Maher, B. C. Thomsen, and I. Darwazeh, "Dual polarization coherent optical spectrally efficient frequency division multiplexing," *IEEE Photon. Technol. Lett.*, vol. 28, no. 1, pp. 83–86, Jan. 1, 2016.

[15] T. Xu, S. Mikroulis, J. E. Mitchell, and I. Darwazeh, "Bandwidth compressed waveform for 60-GHz millimeter-wave radio over fiber experiment," *J. Lightw. Technol.*, vol. 34, no. 14, pp. 3458–3465, Jul. 15, 2016.

[16] S. V. Zavjalov, S. V. Volvenko, and S. B. Makarov, "A method for increasing the spectral and energy efficiency SEFDM signals," *IEEE Commun. Lett.*, vol. 20, no. 12, pp. 2382–2385, Dec. 2016.

[17] J. Zhou *et al.*, "Capacity limit for faster-than-Nyquist non-orthogonal frequency-division multiplexing signaling," *Sci. Rep.*, vol. 7, Jun. 2017, Art. no. 3380.

[18] J. Xu *et al.*, "Narrowband Internet of Things: Evolutions, technologies, and open issues," *IEEE Internet Things J.*, vol. 5, no. 3, pp. 1449–1462, Jun. 2018.

[19] M. R. D. Rodrigues and I. Darwazeh, "Fast OFDM: A proposal for doubling the data rate of OFDM schemes," in *Proc. Int. Conf. Telecommun.*, vol. 3, 2002, pp. 484–487.

[20] T. Xu and I. Darwazeh, "Transmission experiment of bandwidth compressed carrier aggregation in a realistic fading channel," *IEEE Trans. Veh. Technol.*, vol. 66, no. 5, pp. 4087–4097, May 2017.

[21] B. Farhang-Boroujeny, "OFDM versus filter bank multicarrier," *IEEE Signal Process. Mag.*, vol. 28, no. 3, pp. 92–112, May 2011.

[22] N. Michailow *et al.*, "Generalized frequency division multiplexing for 5th generation cellular networks," *IEEE Trans. Commun.*, vol. 62, no. 9, pp. 3045–3061, Sep. 2014.

[23] V. Vakilian, T. Wild, F. Schaich, S. Ten Brink, and J.-F. Frigon, "Universal-filtered multi-carrier technique for wireless systems beyond LTE," in *Proc. IEEE Globecom Workshops (GC Wkshps)*, Dec. 2013, pp. 223–228.

[24] T. Xu and I. Darwazeh, "Nyquist-SEFDM: Pulse shaped multicarrier communication with sub-carrier spacing below the symbol rate," in *Proc. 10th Int. Symp. Commun. Syst. Netw. Digit. Signal Process. (CSNDSP)*, Jul. 2016, pp. 1–6.

[25] J. Proakis and M. Salehi, *Digital Communications*. Boston, MA, USA: McGraw-Hill, 2008.

[26] E. Dahlman, S. Parkvall, and J. Sköld, *4G LTE/LTE-Advanced for Mobile Broadband*. Amsterdam, The Netherlands: Elsevier, 2011.

[27] S. Malkowsky *et al.*, "The worlds first real-time testbed for massive MIMO: Design, implementation, and validation," *IEEE Access*, vol. 5, pp. 9073–9088, 2017.

[28] X. Yang *et al.*, "Design and implementation of a TDD-based 128-antenna massive MIMO prototype system," *China Commun.*, vol. 14, no. 12, pp. 162–187, Dec. 2017.

[29] Y. S. Cho, J. Kim, W. Y. Yang, and C.-G. Kang, *MIMO-OFDM Wireless Communications With MATLAB*. Singapore: Wiley, 2010.

[30] T. Xu, H. Ghannam, and I. Darwazeh, "Practical evaluations of SEFDM: Timing offset and multipath impairments," *Infocommun. J.*, 2019.

[31] Y. Liu, Z. Tan, H. Hu, L. J. Cimini, and G. Y. Li, "Channel estimation for OFDM," *IEEE Commun. Surveys Tuts.*, vol. 16, no. 4, pp. 1891–1908, 4th Quart., 2014.

[32] P. N. Whatmough, M. R. Perrett, S. Isam, and I. Darwazeh, "VLSI architecture for a reconfigurable spectrally efficient FDM baseband transmitter," *IEEE Trans. Circuits Syst. I, Reg. Papers*, vol. 59, no. 5, pp. 1107–1118, May 2012.

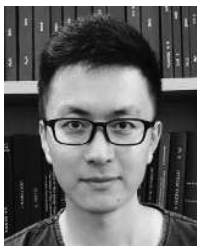

Tongyang Xu (S'13–M'17) received the B.Eng. degree in electronic information engineering from Xidian University, Xi'an, China, in 2011, and the M.Sc. degree (with distinction) in telecommunications and the Ph.D. degree in electronic and electrical engineering from University College London (UCL), London, U.K., in 2012 and 2017, respectively.

He is currently a Senior Research Associate with Communications and Information Systems Group, Department of Electronic and Electrical Engineering, UCL. He has authored or co-authored approximately 40 papers in the areas of wireless and optical communications. He contributed to *Signal Processing for 5G: Algorithms and Implementations* (Wiley, 2016) and *Key Enabling Technologies for 5G Mobile Communications* (Springer, 2016). His current research interests include 5G/B5G communications, waveform design, Internet of Things, software defined radio, real-time testbed prototyping, machine learning, neural networks design, and data analysis.

Dr. Xu was a recipient of the UCL Faculty of Engineering Sciences Scholarship in 2013. He was the nominated investigator of the two successful Impact Acceleration Discovery to Use Awards at UCL in 2016 and 2018 and was a co-recipient of Smart Agriculture Entrepreneurship Grant at Rothamsted Research in 2017, the Chinese Government Award for Outstanding Self-Financed Students Abroad in 2017, the Lombardi Prize runner up for the best Ph.D. thesis in 2018, and the National Instruments Academic Research Grant Award in 2018.

Christos Masouros (M'06–SM'14) received the Diploma degree in electrical and computer engineering from the University of Patras, Patras, Greece, in 2004, and the M.Sc. degree by research and Ph.D. degree in electrical and electronic engineering from the University of Manchester, Manchester, U.K., in 2006 and 2009, respectively.

In 2008, he was a Research Intern with Philips Research Labs, Cambridge, U.K. From 2009 to 2010, he was a Research Associate with the University of Manchester and from 2010 to 2012 a Research Fellow with Queen's University Belfast, Belfast, U.K. In 2012, he joined the University College London, London, U.K., as a Lecturer. He has held a Royal Academy of Engineering Research Fellowship from 2011 to 2016. He is currently an Associate Professor with the Communications and Information Systems research Group, Department of Electrical and Electronic Engineering, University College London. His current research interests include wireless communications and signal processing with particular focus on green communications, large scale antenna systems, cognitive radio, interference mitigation techniques for MIMO, and multicarrier communications.

Dr. Masouros was a recipient of the Best Paper Award of the IEEE GlobeCom 2015 Conference and has been recognized as an Exemplary Editor for IEEE COMMUNICATIONS LETTERS, and as an Exemplary Reviewer for the IEEE TRANSACTIONS ON COMMUNICATIONS. He is an Editor for the IEEE TRANSACTIONS ON COMMUNICATIONS and the IEEE TRANSACTIONS ON WIRELESS COMMUNICATIONS. He has been an Associate Editor for IEEE COMMUNICATIONS LETTERS and a Guest Editor for the IEEE JOURNAL ON SELECTED TOPICS IN SIGNAL PROCESSING issues "Exploiting Interference towards Energy Efficient and Secure Wireless Communications" and "Hybrid Analog/Digital Signal Processing for Hardware-Efficient Large Scale Antenna Arrays." He is currently an elected member of the EURASIP SAT Committee on Signal Processing for Communications and Networking.

Izzat Darwazeh (SM'03) received the graduation degree in electrical engineering from the University of Jordan, Amman, Jordan, in 1984, and the M.Sc. and Ph.D. degrees from the University of Manchester, Manchester, U.K., in 1986 and 1991, respectively.

He holds the University of London Chair of Communications Engineering and leads the 70-Strong Communications and Information Systems Group with the Department of Electronic and Electrical Engineering, University College London (UCL), London, U.K. He is also the Director of the ICCS and the Institute of Communications and Connected Systems, UCL. He has authored or co-authored over 250 papers and book chapters in the areas of optical and wireless communications and monolithic microwave integrated circuits and high-speed/frequency circuits. He co-edited *Analogue Optical Fibre Communications* (IEE, 1995) and was a co-editor of an Elsevier-Newness book on electrical engineering in 2008. He co-authored *Linear Circuit Analysis and Modelling* (Elsevier, 2005) and *Microwave Active Circuit Analysis and Design* (Academic, 2015). He currently teaches mobile and wireless communications and circuit design. In 2002, he proposed (with M. Rodrigues) the Fast OFDM concept and in 2003 the SEFDM concept and has been researching on these topics. His current research interests include ultrahigh-speed microwave circuits and wireless and optical communication systems.

Dr. Darwazeh is a Chartered Engineer and a Fellow of the IET and Institute of Telecommunications Professionals FITP.